HYBRID QUANTUM TRANSFORMER FOR LANGUAGE GENERATION *

Desheng Kong

Nankai University {kongds@mail.nankai.edu.cn}

Xiangshuo Cui

Nankai University {2120250604@mail.nankai.edu.cn}

Jiaying Jin

Nankai University {2120250515@mail.nankai.edu.cn}

Jing Xu

Nankai University {xujing@nankai.edu.cn}

Donglin Wang

Nankai University
Beijing Sursen Information Technology Co., Ltd
{wangdonglin@sursen.net}

ABSTRACT

Although quantum computing has been increasingly applied to replace classical computation, most existing quantum or hybrid models remain confined to simple tasks, with no successful application to large-scale natural language generation to date. In this work, we present the first hybrid quantum—classical large language model (LLM) for natural language generation, HyQuT, capable of performing coherent and context-aware dialogue. The proposed architecture integrates variational quantum circuits (VQCs) into the Transformer framework at both 8M and 150M parameter scales. Experimental results show that a minimal number of qubits (10 qubits with 80 quantum gates) can replace about 10% of the classical parameters in the 150M-parameter model, while achieving comparable convergence stability and generation quality. This study provides an early demonstration of the feasibility of integrating quantum computing to large-scale generative language models.

Keywords Quantum Transformer · Quantum machine learning · Large language models

1 Introduction

Recent advances in Transformer-based large language models (LLMs), beginning with the seminal Transformer architecture[1], have driven remarkable progress in natural language generation. The paradigm of scaling these models, exemplified by landmark architectures like the GPT series[2, 3] and now widely adopted in open-source models such as LLaMA[4], has unlocked unprecedented capabilities. Yet, this continual scaling has led to substantial and often prohibitive computational and energy demands[5]. As model parameters grow into the hundreds of millions or billions, training and inference increasingly strain classical hardware resources, highlighting the urgent need for new computing paradigms to alleviate these bottlenecks. Quantum computing, with its potential for exponential parallelism and compact information representation, has emerged as a promising alternative for enhancing neural architectures[6].

Despite rapid progress in quantum machine learning, most existing quantum or hybrid models remain limited to small-scale tasks such as classification, regression, or time-series forecasting. Their architectures typically involve shallow quantum circuits or isolated quantum layers without integration into large-scale generative models. To date, no study has successfully demonstrated a quantum–classical hybrid model capable of coherent and context-aware language

^{*} Citation: Kong. HyQuT.

generation, leaving an unexplored gap between quantum computation and large-scale natural language processing (NLP).

In this work, we present the first hybrid quantum—classical LLM designed for generative NLP tasks, HyQuT. Our approach explores the feasibility of embedding variational quantum circuits (VQCs) into different layers of Transformer architectures to replace part of the classical linear transformations, thereby reducing parameter redundancy while preserving generative capability. This hybrid integration enables the model to leverage quantum representations for feature projection and contextual reasoning within the Transformer framework.

We evaluate HyQuT at both 8M and 150M parameter scales through pre-training and fine-tuning experiments on high-quality Chinese corpora. Results show that approximately 10% of the classical parameters can be replaced by a minimal number of quantum resources—only 10 qubits with 80 quantum gates—while achieving comparable convergence stability and text generation quality. These findings demonstrate that even under near-term hardware constraints, quantum circuits can provide tangible benefits to large-scale generative models.

In summary, this study contributes (1) the first demonstration of a hybrid quantum—classical large model capable of natural language generation, and (2) empirical evidence that quantum circuits can effectively substitute part of the classical computation in Transformers with reduced parameters and comparable performance, providing a feasible direction for quantum-enhanced NLP models.

2 Related Works

2.1 Large Language Models and the Scaling Paradigm

The foundation of modern NLP was revolutionized by the Transformer architecture, which introduced the self-attention mechanism as a powerful tool for capturing long-range dependencies in text [1]. This design departed from recurrent structures, enabling massive parallelization and paving the way for models of unprecedented scale. Early applications of this architecture, such as BERT [7], demonstrated the power of large-scale pre-training on general language understanding tasks, typically followed by fine-tuning for specific applications.

A subsequent paradigm shift moved towards generative pre-training, where models are trained to predict the next token in a sequence. This approach, championed by the GPT family of models [2, 3], revealed that scaling up model size, dataset size, and compute leads to predictable improvements in performance, a phenomenon formalized as "scaling laws"[8]. These (LLMs) exhibit emergent abilities, allowing them to perform a wide range of tasks with zero or few-shot prompting, without task-specific training. The development of instruction tuning [9] and reinforcement learning from human feedback (RLHF) [10] further refined these models' ability to align with user intent, making them powerful and steerable tools.

The contemporary LLM landscape is characterized by both enormous proprietary models and a burgeoning ecosystem of powerful open-source alternatives like LLaMA and its derivatives [4, 11]. While their capabilities are vast, the immense computational cost remains a central challenge. In response, the classical machine learning community has developed various parameter-efficient fine-tuning (PEFT) techniques, such as LoRA [12], to reduce the cost of adapting these models. While such methods address the adaptation phase, the fundamental cost of pre-training and inference remains. This persistent challenge motivates exploring alternative computational paradigms, such as quantum computing, to fundamentally reimagine the building blocks of these powerful architectures.

2.2 Quantum Natural Language Processing (QNLP)

Quantum Natural Language Processing (QNLP) has emerged as a novel paradigm aiming to leverage the principles of quantum mechanics to model the complexities of human language. Early foundational work in this area, notably the DisCoCat framework, proposed using the compositional structure of quantum tensor networks to represent the grammatical and semantic composition of sentences [13]. This approach holds theoretical appeal, as the high-dimensional Hilbert spaces and phenomena like superposition and entanglement could offer more natural and resource-efficient representations for complex linguistic features, such as semantic ambiguity and logical entailment.

However, these early QNLP models, while theoretically elegant, have largely been confined to syntactic parsing or small-scale semantic classification tasks. Their architectures are typically rigid and task-specific, lacking the scalability and, crucially, the generative capabilities that characterize modern, large-scale language models. To bridge this gap and unlock the potential of QNLP for more complex applications, the research community has increasingly turned its attention toward developing quantum analogues of the highly successful Transformer architecture.

2.3 Quantum Self-Attention and Quantum Transformers

The cornerstone of the Transformer model is its self-attention mechanism. Consequently, the primary challenge in creating a quantum Transformer lies in designing an efficient and physically realizable Quantum Self-Attention (QSA) module. This has spurred a variety of innovative approaches, which, despite their architectural diversity, reveal a striking convergence in their ultimate application goals.

The initial and most direct line of inquiry has focused on creating a quantum analogue of the classical self-attention process. The pioneering QSANN model first introduced a framework where Query, Key, and Value vectors are encoded into parameterized quantum circuits (PQCs), and their inner-product similarity is estimated via quantum measurements [14]. The viability of this core concept was successfully demonstrated on several text classification benchmarks. Following this, a significant body of work has sought to refine and extend this paradigm. These advancements include enhancing measurement schemes to reduce parameter counts [15], incorporating more generalized measurement techniques like POVMs [16], and adapting the architecture for different data modalities. Notably, this QSA mechanism has been extended from its NLP origins to the domains of computer vision [14, 17], high-energy physics [18, 19], and time-series forecasting [20, 21]. These efforts, while expanding the applicability of QSA, have consistently targeted problems of a discriminative nature, where the objective is to classify, predict, or regress a specific output.

A parallel research thrust has explored more sophisticated methods for computing attentional similarity, moving beyond simple inner products. For instance, some models have proposed novel metrics such as quantum logical similarity [22] or complex-valued similarity that leverages the phase information of qubits [23] to capture non-linear relationships between inputs. Other novel designs, such as holistic attention models that bypass explicit score computation [24] have also been proposed. Yet, their evaluation remains within the confines of classification or theoretical analysis.

This comprehensive review reveals an unmistakable pattern: the overwhelming body of research on quantum Transformers is dedicated to discriminative tasks. The fundamental goal of these models is to compress high-dimensional input data into a distilled representation suitable for making a classification or prediction. To the best of our knowledge, the crucial domain of generative tasks, particularly in NLP, remains entirely unexplored. This represents a significant omission, as generative capabilities are a hallmark of modern artificial intelligence and a critical step towards achieving more sophisticated and human-like language understanding and creation.

To address this critical gap, this paper introduces the first quantum Transformer architecture designed and implemented specifically for generative NLP. Our work aims to expand the horizon of QNLP from discriminative modeling to the more challenging and impactful realm of language generation.

3 Method

3.1 Quantum-Classical Hybrid Computational Paradigm Architecture Design

The core of HyQuT is an innovative quantum-classical hybrid module, engineered to function as a direct replacement for standard linear projection layers and to transcend the expressive limitations of classical linear transformations. By deeply integrating a variational quantum circuit into the Transformer architecture, we leverage the intrinsic superposition and entanglement properties of quantum states. This allows the module to operate within and explore a feature space of exponential capacity—a Hilbert space scaling as $\mathcal{O}(2^{n_q})$, where n_q is the number of qubits. This stands in stark contrast to a traditional parameter matrix, such as the Query projection $\mathbf{W}^Q \in \mathbb{R}^{d_{model} \times d_k}$, whose expressive power is constrained by a polynomial number of real-valued parameters. Through this integration, we enable end-to-end differentiable optimization of complex, non-linear feature transformations, creating a theoretical path for quantum-enhanced representation learning in large-scale models.

However, harnessing this theoretical power within a practical hybrid system presents a formidable challenge: the seamless integration of a high-dimensional classical feature space (e.g., a model's hidden dimension of 512) with the constrained, low-dimensional nature of near-term quantum processors (e.g., 10-20 qubits). A naive, direct encoding is infeasible with current hardware and algorithms. To address this challenge, our module introduces a practical and scalable three-stage architecture: (1) a classical dimensionality reduction encoder, (2) a core parameterized quantum circuit, and (3) a classical dimensionality augmentation decoder. This structure effectively bridges the dimensional gap, making the integration of quantum circuits into large-scale models tractable while allowing the entire module to be trained end-to-end within a standard deep learning framework.

In Figure 1, the Hybrid Quantum Module, framed by the orange dotted line, is a general-purpose projection module. It takes a high-dimensional classical vector Input from the Transformer. A Dimensionality Reduction Layer first compresses the input into a low-dimensional representation suitable for the quantum backend. This vector is then encoded into a parameterized quantum circuit, which performs a variational transformation. Finally, the measurement

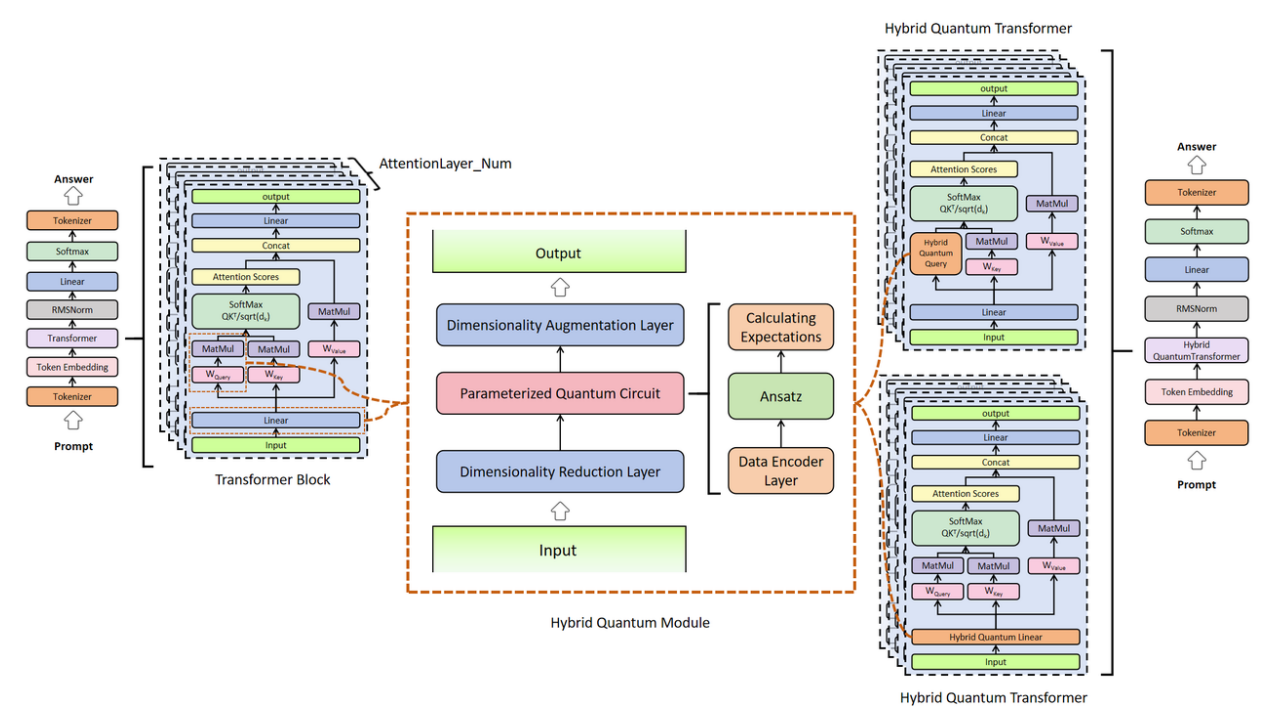


Figure 1: The architecture of the Overall Hybrid Architecture. The framework consists of a general-purpose projection module (middle) and its specific integration into the Transformer architecture (right).

result from the quantum circuit is fed into a Dimensionality Augmentation Layer to project it back to the original hidden dimension, producing the final Output vector. The entire module acts as a drop-in replacement for a classical linear layer. The top-right diagram illustrates the architecture of HyQuT-150M, which replaces the Query projection matrix (W_q) in the self-attention block, while the bottom-right diagram shows the architecture for HyQuT-8M, where the gate projection matrix in the FFN block is replaced.

3.2 Quantum-Adaptive Dimensionality Reduction for High-Dimensional Semantic Space

Given the input semantic representation tensor $\mathbf{X}^{(\ell)} \in \mathbb{R}^{B \times L \times d_{model}}$ at the ℓ -th Transformer layer, where $B \in \mathbb{Z}^+$ represents the mini-batch training sample size, $L \in \mathbb{Z}^+$ denotes the input sequence token length, and $d_{model} \in \mathbb{Z}^+$ indicates the Transformer hidden layer feature dimension. To achieve effective mapping from classical high-dimensional feature spaces to quantum Hilbert spaces, we introduce an Adaptive Feature Compression Module that projects semantic vectors into quantum circuit-processable subspaces through learnable affine transformations:

$$\mathbf{X}_{compressed}^{(\ell)} = \sigma_{compress} \left(\mathbf{X}^{(\ell)} \mathbf{W}_{down}^{(\ell)} + \mathbf{b}_{down}^{(\ell)} \right)$$
(1)

where the dimensionality reduction projection matrix $\mathbf{W}_{down}^{(\ell)} \in \mathbb{R}^{d_{model} \times 2n_q}$ and bias vector $\mathbf{b}_{down}^{(\ell)} \in \mathbb{R}^{2n_q}$ are trainable parameters for this layer, and $\sigma_{compress}(\cdot)$ is the Tanh activation function ensuring feature value boundedness. The compressed tensor $\mathbf{X}_{compressed}^{(\ell)} \in \mathbb{R}^{B \times L \times 2n_q}$ preserves the core information entropy of the original semantic representation while reducing dimensionality to a $2n_q$ -dimensional submanifold matching quantum encoding requirements.

The $2n_q$ -dimensional design is based on the dual degree-of-freedom requirement for quantum state encoding: each qubit requires two independent rotation angle parameters (θ, ϕ) to fully determine its quantum state on the Bloch sphere. This design ensures injective mapping from classical information to quantum states, preventing information loss.

3.3 Tensor Reconstruction Operator for Quantum Circuit Batch Processing

To enable efficient batched processing of quantum circuits, we define a tensor reconstruction operator \mathcal{T}_{batch} : $\mathbb{R}^{B \times L \times 2n_q} \to \mathbb{R}^{(B \cdot L) \times 2n_q}$ that merges the batch and sequence dimensions into a unified quantum circuit parallel

processing dimension:

$$\mathbf{X}_{flat}^{(\ell)} = \mathcal{T}_{batch}(\mathbf{X}_{compressed}^{(\ell)}) = \text{Flatten}_{[0,1]}(\mathbf{X}_{compressed}^{(\ell)})$$
 (2)

where $\mathrm{Flatten}_{[0,1]}(\cdot)$ denotes the tensor reorganization operation flattening along the first two dimensions. The transformed $\mathbf{X}_{flat}^{(\ell)} \in \mathbb{R}^{(B \cdot L) \times 2n_q}$ can be viewed as $N_{batch} = B \cdot L$ independent quantum circuit input instances, each carrying $2n_q$ classical feature values to be encoded into quantum states. This tensor reconstruction strategy fully exploits the parallelism of quantum circuit execution, enabling a single quantum computation to simultaneously process all time steps across the entire batch and sequence, significantly enhancing computational efficiency.

3.4 Parameterized Quantum State Encoding Protocol

For the *i*-th input instance $\mathbf{x}_i = [x_{i,1}, x_{i,2}, \dots, x_{i,2n_q}]^T \in \mathbb{R}^{2n_q}$ where $i \in 1, 2, \dots, N_{batch}$, we construct a quantum register containing n_q qubits and employ a three-stage parameterized encoding protocol to map classical features to quantum states. Two quantum circuits used in the model are shown in Figure 2, with Figure 2b as an example.

3.4.1 Stage I: Uniform Initialization of Quantum State Space

The quantum register is initialized to the ground state $|0\rangle^{\otimes n_q}$, followed by application of Hadamard gates H to all qubits to construct a uniform superposition of maximally mixed states:

$$|\psi_0\rangle = \mathcal{H}^{\otimes n_q}|0\rangle^{\otimes n_q} = \bigotimes_{j=1}^{n_q} \frac{1}{\sqrt{2}}(|0\rangle_j + |1\rangle_j) = \frac{1}{\sqrt{2^{n_q}}} \sum_{k=0}^{2^{n_q}-1} |k\rangle$$
 (3)

where ${\cal H}$ represents the Hadamard gate operator, defined as:

$$H = \frac{1}{\sqrt{2}} \begin{pmatrix} 1 & 1\\ 1 & -1 \end{pmatrix} \tag{4}$$

This initialization creates an equal-probability quantum superposition of 2^{n_q} computational basis states, providing maximal state space exploration potential for subsequent feature encoding and embodying the essential advantage of quantum parallelism.

3.4.2 Stage II: Angular Embedding for Feature Encoding

For qubit $j \in 1, 2, ..., n_q$, parameterized rotation gates $R_Y(\theta_j)$ and $R_Z(\phi_j)$ are sequentially applied around the Y and Z axes, implementing dual-channel encoding of classical features into quantum state amplitudes and phases:

$$R_Y(\theta) = \exp\left(-i\frac{\theta}{2}\hat{\sigma}_y\right) = \begin{pmatrix} \cos(\theta/2) & -\sin(\theta/2) \\ \sin(\theta/2) & \cos(\theta/2) \end{pmatrix}$$
 (5)

$$R_Z(\phi) = \exp\left(-i\frac{\phi}{2}\hat{\sigma}_z\right) = \begin{pmatrix} e^{-i\phi/2} & 0\\ 0 & e^{i\phi/2} \end{pmatrix} \tag{6}$$

where $\hat{\sigma}_y$, $\hat{\sigma}_z$ are Pauli operators. Rotation angles are extracted from input features through nonlinear mapping functions:

$$\theta_i = \pi \cdot \sigma(x_{i,j}), \quad \phi_i = \pi \cdot \sigma(x_{i,n_q+j})$$
 (7)

Here $\sigma(z) = (1 + e^{-z})^{-1}$ is the Sigmoid function with range [0,1], scaled by π to ensure rotation angles lie within the $[0,\pi]$ interval, covering the southern hemisphere of the Bloch sphere and providing sufficient state space representational capacity.

3.4.3 Stage III: Quantum Superposition of Encoded States

After completing angular encoding, the quantum state corresponding to the i-th input instance is the tensor product of individual qubit encoded states:

$$\left|\psi_{\text{enc}}^{(i)}\right\rangle = \bigotimes_{j=1}^{n_q} R_Z(\phi_j) R_Y(\theta_j) H \left|0\right\rangle_j \tag{8}$$

This quantum state forms a high-dimensional quantum embedding of the input features in the 2^{n_q} -dimensional Hilbert space $\mathcal{H}^{\otimes n_q}$, with its state vector containing 2^{n_q} complex amplitude components, far exceeding the information capacity of classical $2n_q$ -dimensional inputs and demonstrating the exponential expressive advantage of quantum encoding.

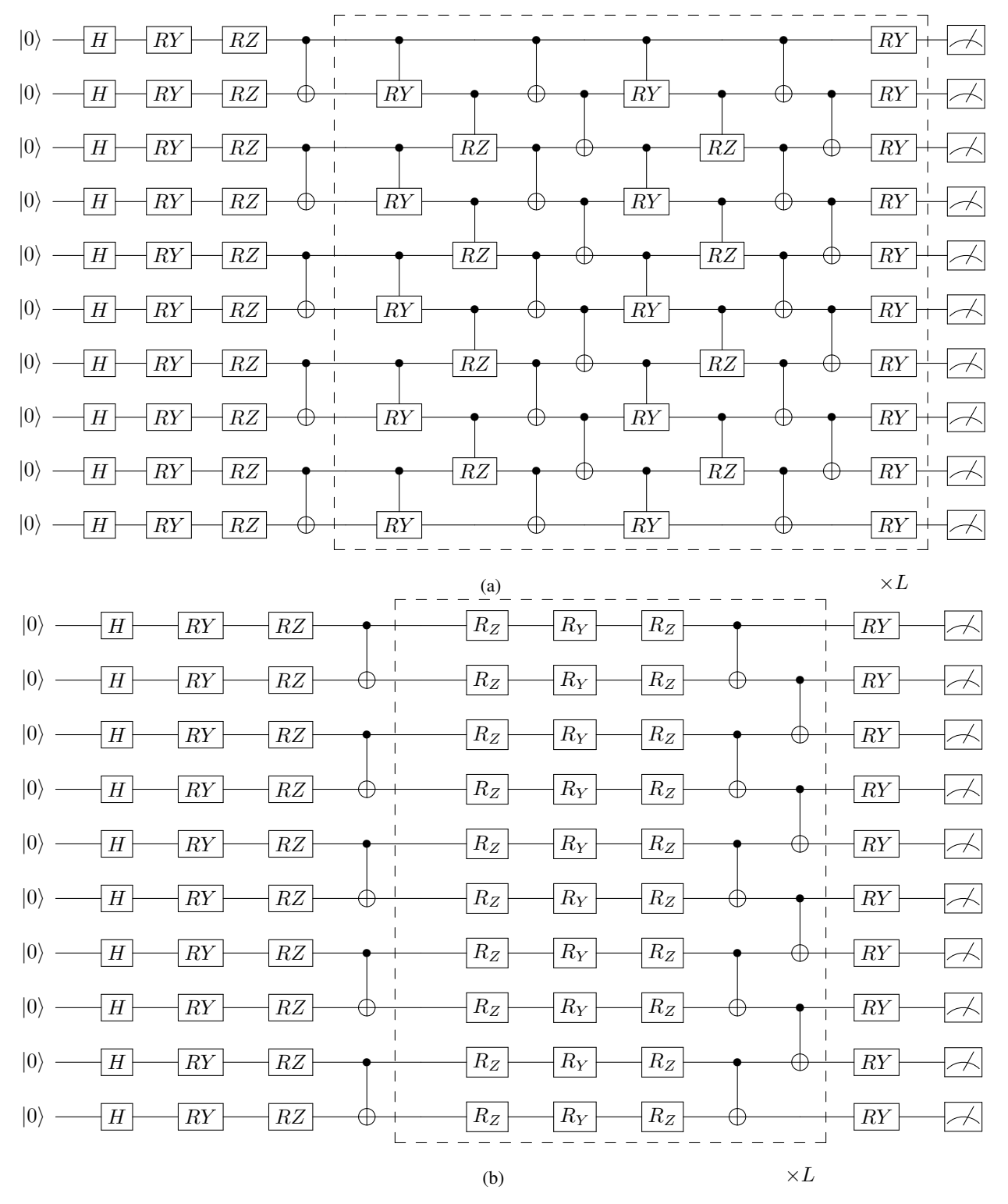


Figure 2: A schematic diagram of quantum circuits, where (a) is the quantum circuit of the HyQuT-8M model and (b) is the quantum circuit of the HyQuT-150M. The main difference between the two is the entanglement strength of the variable quantum parameters and the type of rotating gate.

3.5 Hierarchical Variational Quantum Feature Transformation

The encoded quantum state undergoes deep feature extraction and nonlinear transformation through $N_L \in \{2,3\}$ layers of parameterized Ansatz circuits. Each Ansatz layer constitutes a unitary transformation operator, with design following the Hardware-Efficient Ansatz paradigm, balancing expressive power and near-term quantum device realizability.

3.5.1 Unitary Decomposition of Single-Layer Ansatz

The ℓ -th layer Ansatz operator $U_{\text{ansatz}}^{(\ell)}: \mathcal{H}^{\otimes n_q} \to \mathcal{H}^{\otimes n_q}$ can be decomposed into the composition of a parameterized rotation layer $U_{\text{rot}}^{(\ell)}$ and an entangling gate layer $U_{\text{ent}}^{(\ell)}$:

$$U_{\text{ansatz}}^{(\ell)} = U_{\text{ent}}^{(\ell)} \circ U_{\text{rot}}^{(\ell)} \tag{9}$$

The parameterized rotation layer consists of independent three-rotation gate sequences on each qubit:

$$U_{\text{rot}}^{(\ell)} = \bigotimes_{j=1}^{n_q} R_Z(\alpha_j^{(\ell)}) R_Y(\beta_j^{(\ell)}) R_Z(\gamma_j^{(\ell)})$$
(10)

where the variational parameter set $\Theta^{(\ell)} = \{\alpha_j^{(\ell)}, \beta_j^{(\ell)}, \gamma_j^{(\ell)}\}_{j=1}^{n_q}$ is optimized through end-to-end training. This ZYZ decomposition enables universal approximation of arbitrary single-qubit unitary gates on the Bloch sphere, ensuring expressive completeness at the single-qubit level.

3.5.2 Quantum Entanglement Induction Mechanism

The entangling gate layer $U_{\text{ent}}^{(\ell)}$ establishes quantum correlations between adjacent qubits through controlled-NOT (CNOT) gates:

$$U_{\text{ent}}^{(\ell)} = \prod_{j=1}^{n_q} \text{CNOT}_{j \to [(j \bmod n_q) + 1]}$$

$$\tag{11}$$

where $CNOT_{c \to t}$ denotes a controlled-NOT gate with control qubit c acting on target qubit t, with matrix representation:

$$CNOT = |0\rangle \langle 0| \otimes \mathbb{I} + |1\rangle \langle 1| \otimes \hat{X} = \begin{pmatrix} 1 & 0 & 0 & 0 \\ 0 & 1 & 0 & 0 \\ 0 & 0 & 0 & 1 \\ 0 & 0 & 1 & 0 \end{pmatrix}$$
 (12)

The circular connectivity topology $(1 \to 2 \to \cdots \to n_q \to 1)$ ensures global information propagation among all qubits, generating multipartite entangled states. Quantum entanglement causes the system's joint state to be non-decomposable into simple tensor products of subsystem states, producing nonlocal quantum correlations that transcend classical correlations—a key source of quantum neural network expressive power.

3.5.3 Deep Quantum Evolution

After N_L cascaded transformations, the final quantum state is:

$$\left|\psi_{\text{final}}^{(i)}\right\rangle = \mathcal{U}_{\text{VQC}}(\Theta)\left|\psi_{\text{enc}}^{(i)}\right\rangle = \left(\prod_{\ell=1}^{N_L} U_{\text{ansatz}}^{(\ell)}\right)\left|\psi_{\text{enc}}^{(i)}\right\rangle \tag{13}$$

where $\mathcal{U}_{\text{VQC}}(\Theta)$ represents the complete VQC unitary operator, and $\Theta = \bigcup_{\ell=1}^{N_L} \Theta^{(\ell)}$ encompasses all variational parameters across layers. According to the Solovay-Kitaev theorem, as layer number N_L increases and parameter count expands, this hierarchical unitary circuit can approximate arbitrary unitary transformations in the $SU(2^{n_q})$ group with arbitrary precision, endowing VQCs with powerful function approximation capabilities.

The quantum circuit depth N_L selection balances expressive power and training complexity: $N_L=2$ layers can establish fundamental quantum entanglement structures, while $N_L=3$ layers further enhance nonlinear modeling capabilities through additional parameterized degrees of freedom, while controlling gradient computation circuit execution costs.

3.6 Quantum Observable Measurement and Expectation Value Extraction

To extract classical information from evolved quantum states for subsequent neural network computation, we perform projective measurements based on Pauli-Z operators on each qubit and compute measurement operator quantum expectation values as output features.

3.6.1 Construction of Local Observables

For the *j*-th qubit, define the local measurement operator as:

$$\hat{O}_{i} = \mathbb{I}^{\otimes (j-1)} \otimes \hat{\sigma}_{z}^{(j)} \otimes \mathbb{I}^{\otimes (n_{q}-j)} \tag{14}$$

where the Pauli-Z operator $\hat{\sigma}_z = |0\rangle \langle 0| - |1\rangle \langle 1|$ has eigenvalues $\{+1, -1\}$, corresponding to the qubit being in states $|0\rangle$ and $|1\rangle$ respectively. This diagonalized operator choice enables measurement expectation values to be computed via probability weighting:

$$m_j^{(i)} = \left\langle \psi_{\text{final}}^{(i)} \middle| \hat{O}_j \middle| \psi_{\text{final}}^{(i)} \right\rangle = P_0^{(j)} - P_1^{(j)}$$
 (15)

where $P_0^{(j)}, P_1^{(j)}$ are the probabilities of measuring the j-th qubit in states $|0\rangle, |1\rangle$ respectively. The expectation value $m_j^{(i)} \in [-1, +1]$ encodes statistical information about that qubit's state: $m_j \approx +1$ indicates primarily in state $|0\rangle, m_j \approx -1$ indicates primarily in state $|1\rangle$, and $m_j \approx 0$ indicates a maximally mixed state.

3.6.2 Batched Measurement Protocol

Performing parallel measurements on all n_q qubits constitutes the output vector for the i-th circuit instance:

$$\mathbf{m}^{(i)} = \begin{bmatrix} m_1^{(i)} \\ m_2^{(i)} \\ \vdots \\ m_{n_q}^{(i)} \end{bmatrix} = \begin{bmatrix} \langle \hat{O}_1 \rangle | \psi_{\text{final}}^{(i)} \rangle \\ \langle \hat{O}_2 \rangle | \psi_{\text{final}}^{(i)} \rangle \\ \vdots \\ \langle \hat{O}_{n_q} \rangle | \psi_{\text{final}}^{(i)} \rangle \end{bmatrix} \in \mathbb{R}^{n_q}$$

$$(16)$$

Executing the above measurement process on all $N_{\text{batch}} = B \cdot L$ quantum circuit instances yields the batched output matrix:

$$\mathbf{M}_{\text{flat}}^{(\ell)} = \begin{bmatrix} (\mathbf{m}^{(1)})^T \\ (\mathbf{m}^{(2)})^T \\ \vdots \\ (\mathbf{m}^{(N_{\text{batch}})})^T \end{bmatrix} \in \mathbb{R}^{(B \cdot L) \times n_q}$$
(17)

Each row of this matrix corresponds to quantum feature representations for a timestep-sample pair, containing n_q -dimensional quantum measurement statistics that encapsulate high-order feature information processed through quantum entanglement and interference.

3.7 Inverse Tensor Reconstruction and Feature Space Upscaling

To re-embed quantum measurement results into the Transformer's sequential structure, we define an inverse tensor reconstruction operator $\mathcal{T}_{\text{batch}}^{-1}: \mathbb{R}^{(B \cdot L) \times n_q} \to \mathbb{R}^{B \times L \times n_q}$ that restores the separated batch and sequence dimensions:

$$\mathbf{M}^{(\ell)} = \mathcal{T}_{\text{hatch}}^{-1}(\mathbf{M}_{\text{flat}}^{(\ell)}) = \text{Unflatten}_{[0 \to (0,1)]}(\mathbf{M}_{\text{flat}}^{(\ell)}, (B, L))$$
(18)

where $Unflatten(\cdot)$ denotes the tensor inverse operation reorganizing flattened dimensions into specified shapes.

Subsequently, an Adaptive Feature Expansion Module projects quantum outputs back to the original hidden layer dimension through learnable linear transformations and nonlinear activations:

$$\mathbf{Q}^{(\ell)} = \text{GELU}\left(\mathbf{M}^{(\ell)}\mathbf{W}_{\text{up}}^{(\ell)} + \mathbf{b}_{\text{up}}^{(\ell)}\right)$$
(19)

where the upscaling projection matrix $\mathbf{W}_{\mathrm{up}}^{(\ell)} \in \mathbb{R}^{n_q \times d_{\mathrm{model}}}$ and bias vector $\mathbf{b}_{\mathrm{up}}^{(\ell)} \in \mathbb{R}^{d_{\mathrm{model}}}$ are trainable parameters for this layer. The GELU (Gaussian Error Linear Unit) activation function is defined as:

$$GELU(x) = x \cdot \Phi(x) = x \cdot \frac{1}{2} \left[1 + erf\left(\frac{x}{\sqrt{2}}\right) \right]$$
 (20)

where $\Phi(\cdot)$ is the cumulative distribution function of the standard normal distribution, and $\operatorname{erf}(\cdot)$ is the error function. GELU provides smooth nonlinear activation, facilitating gradient flow and feature learning. The final Query representation $\mathbf{Q}^{(\ell)} \in \mathbb{R}^{B \times L \times d_{\operatorname{model}}}$ completely replaces the traditional self-attention mechanism's linear projection $\mathbf{Q} = \mathbf{X}\mathbf{W}^Q$, while injecting quantum-processed high-order nonlinear features.

3.8 Quantum-Enhanced Multi-Head Self-Attention Mechanism

The complete quantum-classical hybrid self-attention computational flow integrates quantum feature transformation with classical attention weight computation:

3.8.1 Query-Key-Value Triplet Generation

$$\mathbf{Q}^{(\ell)} = \mathcal{U}_{VQC}(\mathbf{X}^{(\ell)}; \Theta_{VQC}^{(\ell)}) \tag{21a}$$

$$\mathbf{K}^{(\ell)} = \mathbf{X}^{(\ell)} \mathbf{W}_K^{(\ell)} + \mathbf{b}_K^{(\ell)} \tag{21b}$$

$$\mathbf{V}^{(\ell)} = \mathbf{X}^{(\ell)} \mathbf{W}_V^{(\ell)} + \mathbf{b}_V^{(\ell)}$$
(21c)

where $\mathcal{U}_{VQC}(\cdot;\Theta_{VQC})$ represents the complete variational quantum circuit transformation pipeline (including dimensionality reduction, quantum encoding, Ansatz evolution, measurement, and upscaling), and $\Theta_{VQC}^{(\ell)}$ encompasses all trainable parameters related to quantum circuits for this layer. Key and Value maintain classical linear projections to balance computational efficiency with quantum enhancement benefits.

3.8.2 Scaled Dot-Product Attention

Computing attention score matrices based on quantum-generated Query and classical Key:

$$\mathbf{A}^{(\ell)} = \operatorname{softmax} \left(\frac{\mathbf{Q}^{(\ell)} (\mathbf{K}^{(\ell)})^T}{\sqrt{d_k}} + \mathbf{M}_{\text{mask}} \right)$$
 (22)

where $d_k = d_{\text{model}}/h$ is the dimension per attention head, h is the number of heads, and \mathbf{M}_{mask} is the causal mask matrix (for Decoder-Only architectures). Softmax normalization ensures attention weights \mathbf{A}_{ij} satisfy probability distribution constraints $\sum_i A_{ij} = 1$.

The attention-weighted output is:

$$\mathbf{O}_{\text{single}}^{(\ell)} = \mathbf{A}^{(\ell)} \mathbf{V}^{(\ell)} \in \mathbb{R}^{B \times L \times d_k}$$
(23)

3.8.3 Multi-Head Parallelization and Fusion

Extending to h independent quantum-classical hybrid attention heads, where each head $i \in \{1, ..., h\}$ maintains independent quantum circuit parameters $\Theta_{\text{VOC},i}^{(\ell)}$ and projection matrices $\{\mathbf{W}_{K,i}^{(\ell)}, \mathbf{W}_{V,i}^{(\ell)}\}$:

$$head_{i} = Attention\left(\mathcal{U}_{VQC,i}(\mathbf{X}^{(\ell)}), \mathbf{X}^{(\ell)}\mathbf{W}_{K,i}^{(\ell)}, \mathbf{X}^{(\ell)}\mathbf{W}_{V,i}^{(\ell)}\right)$$
(24)

Multi-head outputs are aggregated through concatenation and linear transformation:

$$MultiHead(\mathbf{X}^{(\ell)}) = Concat(head_1, head_2, \dots, head_h)\mathbf{W}_O^{(\ell)}$$
(25)

where $\mathbf{W}_O^{(\ell)} \in \mathbb{R}^{d_{\text{model}} \times d_{\text{model}}}$ is the output projection matrix. The multi-head mechanism enables the model to attend in parallel to different quantum feature subspaces of the input sequence, enhancing representation diversity and robustness.

3.9 Deep Transformer Layer Residual Connections and Normalization

The complete quantum-enhanced Transformer layer follows a Post-LayerNorm architecture, incorporating residual connections to mitigate gradient vanishing in deep networks:

$$\tilde{\mathbf{X}}^{(\ell)} = \mathbf{X}^{(\ell)} + \text{Dropout}\left(\text{MultiHead}(\text{LayerNorm}(\mathbf{X}^{(\ell)}))\right)$$
(26a)

$$\mathbf{X}^{(\ell+1)} = \tilde{\mathbf{X}}^{(\ell)} + \text{Dropout}\left(\text{FFN}(\text{LayerNorm}(\tilde{\mathbf{X}}^{(\ell)}))\right) \tag{26b}$$

where the feedforward network FFN adopts a two-layer fully-connected structure:

$$FFN(\mathbf{X}) = GELU(\mathbf{X}\mathbf{W}_1 + \mathbf{b}_1)\mathbf{W}_2 + \mathbf{b}_2$$
(27)

Layer normalization independently standardizes each sample, with computation formula:

$$LayerNorm(\mathbf{x}) = \frac{\mathbf{x} - \mu}{\sqrt{\sigma^2 + \epsilon}} \odot \gamma + \beta$$
 (28)

where μ , σ^2 are the mean and variance of that sample's features, γ , β are learnable scaling and shift parameters, and ϵ is a numerical stability constant.

Stacking N_{layers} such quantum-enhanced Transformer layers constitutes the complete quantum-classical hybrid LLM backbone network:

$$\mathbf{H} = \mathcal{F}_{\text{Transformer}}(\mathbf{X}^{(0)}) = \left(\prod_{\ell=N_{\text{layers}}}^{1} \mathcal{F}_{\text{layer}}^{(\ell)}\right) (\mathbf{X}^{(0)})$$
(29)

where $\mathbf{X}^{(0)}$ is the input embedding layer output and \mathbf{H} is the final hidden state representation.

3.10 End-to-End Training and Quantum Gradient Computation

The model employs an end-to-end supervised learning paradigm, jointly optimizing quantum circuit variational parameters Θ_{VQC} and classical neural network parameters $\Theta_{\text{classical}}$ through backpropagation algorithms. The training objective is to minimize the cross-entropy loss function for language modeling:

$$\mathcal{L}(\Theta_{\text{VQC}}, \Theta_{\text{classical}}) = -\frac{1}{N_{\text{samples}}} \sum_{i=1}^{N_{\text{samples}}} \sum_{t=1}^{L_i} \sum_{k=1}^{V} y_{i,t,k} \log \hat{p}_{i,t,k}$$
(30)

where N_{samples} is the number of training samples, L_i is the sequence length of the i-th sample, V is the vocabulary size, $y_{i,t,k} \in \{0,1\}$ is the one-hot encoded ground truth label, and $\hat{p}_{i,t,k}$ is the model-predicted vocabulary probability distribution.

3.10.1 Finite Difference Approximation for Quantum Gradients

Due to the nonlinearity of quantum circuits and probabilistic nature of measurements, gradients of quantum parameters $\theta \in \Theta_{VQC}$ cannot be directly obtained through classical automatic differentiation. We employ the Central Finite Difference method for numerical gradient estimation:

$$\frac{\partial \mathcal{L}}{\partial \theta_j} \approx \frac{\mathcal{L}(\theta_j + \delta) - \mathcal{L}(\theta_j - \delta)}{2\delta} \tag{31}$$

where $\delta > 0$ is a small perturbation step size, practically chosen as $\delta \in [10^{-4}, 10^{-3}]$ to balance numerical precision and roundoff errors. Central differences possess $\mathcal{O}(\delta^2)$ truncation error accuracy compared to forward differences, but require two additional quantum circuit forward executions.

For quantum circuits containing $|\Theta_{VQC}|$ variational parameters, complete gradient computation requires $2|\Theta_{VQC}|$ circuit evaluations, with total computational complexity $\mathcal{O}(|\Theta_{VQC}| \cdot T_{circuit})$, where $T_{circuit}$ is the single circuit execution time. Despite introducing constant factors compared to the parameter-shift rule, the finite difference method's implementation simplicity and universality for arbitrary quantum gates provide advantages in practical deployment.

3.10.2 Hybrid Optimization Strategy

The Adam (Adaptive Moment Estimation) optimizer is employed for parameter updates, combining momentum methods with adaptive learning rate adjustments:

$$\mathbf{m}_{t} = \beta_{1} \mathbf{m}_{t-1} + (1 - \beta_{1}) \mathbf{g}_{t}$$

$$\mathbf{v}_{t} = \beta_{2} \mathbf{v}_{t-1} + (1 - \beta_{2}) \mathbf{g}_{t}^{2}$$

$$\hat{\mathbf{m}}_{t} = \mathbf{m}_{t} / (1 - \beta_{1}^{t})$$

$$\hat{\mathbf{v}}_{t} = \mathbf{v}_{t} / (1 - \beta_{2}^{t})$$

$$\theta_{t} = \theta_{t-1} - \eta_{t} \frac{\hat{\mathbf{m}}_{t}}{\sqrt{\hat{\mathbf{v}}_{t}} + \epsilon}$$
(32)

where \mathbf{g}_t is the gradient at step t, \mathbf{m}_t , \mathbf{v}_t are first and second moment estimates of gradients respectively, $\beta_1 = 0.9$, $\beta_2 = 0.999$ are exponential decay rates, and $\epsilon = 10^{-8}$ is a numerical stability term. Bias correction terms $\hat{\mathbf{m}}_t$, $\hat{\mathbf{v}}_t$ compensate for bias in moment estimates during initial stages.

Table 1: Hyperparameters of Classical Baseline Models

Hyperparameter	Classic-8M	Classic-150M
hidden_size	512	1024
num_hidden_layers	2	16
num_attention_heads	8	8
num_key_value_heads	2	2
intermediate_size	1024	2048
max_position_embeddings	4096	32768
seq_len	512	512

3.10.3 Cosine Annealing Learning Rate Schedule

The learning rate η_t adopts a Cosine Annealing with Warm Restarts strategy:

$$\eta_t = \eta_{\min} + \frac{1}{2} (\eta_{\max} - \eta_{\min}) \left(1 + \cos \left(\frac{T_{\text{cur}}}{T_{\max}} \pi \right) \right)$$
 (33)

where $\eta_{\rm max}$ is the maximum learning rate (initial learning rate), $\eta_{\rm min}$ is the minimum learning rate, $T_{\rm cur}$ is the current training step within the period, and $T_{\rm max}$ is the total steps in a single annealing cycle. This strategy smoothly decays the learning rate from $\eta_{\rm max}$ to $\eta_{\rm min}$ during training, then restarts to $\eta_{\rm max}$ periodically, facilitating escape from local optima and exploration of broader parameter spaces—particularly effective for the non-convex optimization landscape of quantum-classical hybrid systems.

Linear warmup is employed in early training, linearly increasing the learning rate from 0 to η_{max} over the first T_{warmup} steps:

$$\eta_t = \eta_{\text{max}} \cdot \frac{t}{T_{\text{warmup}}}, \quad t \le T_{\text{warmup}}$$
(34)

The warmup phase mitigates training instability caused by improper quantum parameter initialization, establishing a solid foundation for subsequent optimization.

4 Experiments

4.1 Experimental Setup

To rigorously evaluate the performance, efficiency, and stability of HyQuT, we conducted a series of experiments across two distinct model scales. We instantiated two primary hybrid model configurations, each targeting a different strategic location within the Transformer architecture, and compared them against their corresponding pure classical baselines. The first configuration, HyQuT-8M, was developed on an 8-million-parameter scale model where the VQC module replaces the gate projection matrix within the Feed-Forward Network. The second, HyQuT-150M, was implemented on a larger 150-million-parameter model, with the VQC module replacing the Query (W_q) projection matrix in the self-attention block. These two configurations allowed us to assess our framework's viability for both rapid prototyping and in more realistic, large-scale settings. The key hyperparameters for their respective classical baselines, Classic-8M and Classic-150M, are detailed in Table 1.

The models were pre-trained on a 1.6 GB Chinese text corpus, which was curated from the Jiangshu Large Model Dataset [25] and filtered for sequences shorter than 512 characters. The pre-training was conducted on a single server equipped with eight H20 GPUs, using a batch size of 32 for a total of 5 epochs (27,585 steps). To ensure stable convergence, we employed a learning rate schedule featuring an initial warm-up phase, a stable plateau, and a final cosine decay.

To provide a comprehensive assessment, our evaluation was structured around three key criteria. First, we measured Resource Efficiency by quantifying the total number of trainable parameters and the theoretical computational cost in Floating-Point Operations (FLOPs). Second, we analyzed the Training Dynamics by examining the pre-training loss curve of each model to evaluate its convergence behavior and stability. Finally, to determine practical performance, we assessed the Generative Quality of the models through a qualitative analysis of their text generation capabilities, focusing on the coherence, context-awareness, and overall quality of the responses.

Replacement Target Parameters (M) FLOPs (B) **Classical Computation (%)** Converged None (Classical Baseline) 7.748 760.3 100.00 $\begin{array}{l} \text{Attention: } W_q \\ \text{Attention: } W_q, W_k, W_v \\ \text{Attention: } W_q, W_k, W_v, W_o \end{array}$ 7.246 710.8 93.49 7.032 689.1 90.64 6.525 639.7 84.14 FFN: W_{gate} 6.722 657.5 86.48 FFN: W_{gate} , W_{up} , W_{down} 4.690 459.6 60.45 All Linear Layers 3.466 339.0 44.59

Table 2: Ablation Study on VQC Replacement Strategies in HyQuT-8M

4.2 Ablation Study on Replacement Strategy

To identify the most effective and stable integration points for the VQC module, we conducted a comprehensive ablation study on the Classic-8M model. The primary goal of this investigation was to understand the sensitivity of the Transformer architecture to the replacement of its various linear layers and to determine the threshold beyond which training stability is compromised. This study allowed us to systematically map out the trade-offs between parameter reduction and model convergence, providing an empirical basis for our main experimental design.

The results of this study are summarized in Table 2. We systematically replaced individual and combined linear layers within both the self-attention and feed-forward network blocks and monitored the model's ability to converge. The parameter count and the estimated Floating-Point Operations (FLOPs) were also calculated for each configuration to quantify the resource savings. To provide a reasonable estimate for the HyQuT-8M (Gate) configuration, its FLOPs were approximated by substituting the VQC with a classical dense layer of equivalent input-output dimensions.

As the results in Table 2 clearly indicate, a distinct pattern emerged regarding training stability. The model successfully converged when individual, functionally critical matrices such as the Query (W_q) or the FFN's Gate (W_{gate}) were replaced. Even a combined replacement of the Query, Key, and Value matrices in the attention block maintained convergence. However, more aggressive strategies that targeted the entire set of linear layers within a functional block—such as all four attention matrices or all three FFN matrices—consistently led to training instability and a failure to converge. This empirical evidence suggests that while the Transformer architecture is robust enough to accommodate a targeted, 'surgical' integration of quantum circuits, its core computational mechanisms are sensitive to large-scale, simultaneous substitutions. These findings strongly informed our decision to focus on the two most promising and stable configurations—replacing the FFN Gate for the HyQuT-8M model and the Attention Query for the HyQuT-150M model—for our main, in-depth analysis.

4.3 Core Results and Analysis

Following the experimental plan, we conducted a detailed analysis of the hybrid models' performance against their classical baselines. The core results confirm that our hybrid quantum-classical framework can achieve significant resource savings without compromising training stability or the ultimate quality of language generation.

A primary motivation for this work is to reduce the classical computational resources required by LLMs. We quantified this by comparing the parameter counts and theoretical FLOPs of our hybrid models against their classical counterparts. As detailed in Table 3, both hybrid configurations demonstrated notable efficiency gains. The HyQuT-8M model, for instance, lowered the classical computational workload of the 8M-scale baseline by over 13.5%, with a corresponding decrease in classical FLOPs. For a complete, layer-by-layer breakdown of the parameter distribution along with the memory usage within the HyQuT-8M model, providing full architectural transparency, please refer to Appendix A.

A critical test for any hybrid architecture is its ability to integrate into the training process and achieve stable convergence. We monitored the pre-training loss curves for both our hybrid models to assess this stability, with the results presented in Figure 3 and Figure 4. Both models demonstrated smooth and successful learning trajectories, confirming the viability of our approach.

At the 8M scale, the HyQuT-8M model exhibits a consistent decrease in loss, starting from an initial value of approximately 8.0 and steadily converging to a final value near 4.0. This positive result was successfully replicated at a much larger scale. The HyQuT-150M model also shows excellent convergence stability. As would be expected for a model with significantly greater capacity, it achieves an even lower final loss, converging to a value of approximately 3.0.

Table 3: Resource	Efficiency	Comparisor	for Hy	brid and	Classical Models
Table 5. Resource	Elliciency	Companison	погпу	bila alla	Ciassical Middels

Model Configuration	Parameters (M)	Parameter Reduction (%)	FLOPs (T)
Classic-150M	149	10.7	14.66
HyQuT-150M	133		13.02
Classic-8M	7.75	13.3	0.76
HyQuT-8M	6.72		0.66

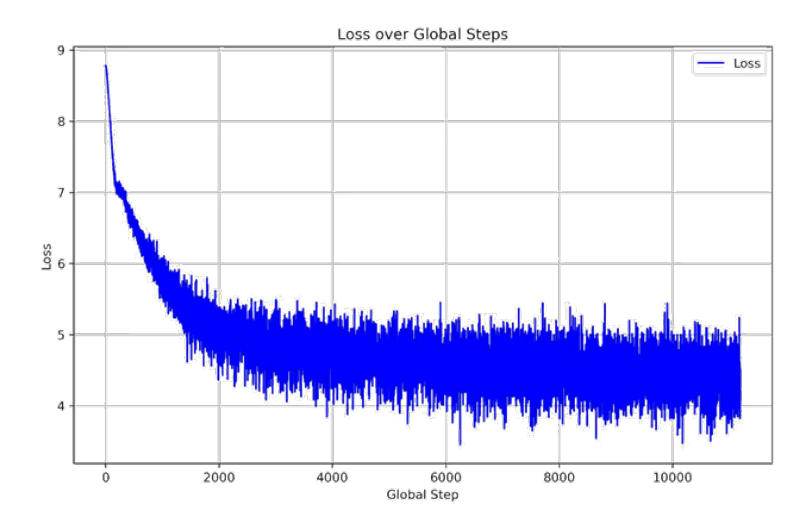


Figure 3: Loss Curve of HyQuT-8M

The successful and stable convergence of both models provides strong evidence that our hybrid module integrates seamlessly into the standard backpropagation-based optimization process. The fact that the framework facilitates effective learning without disruption at both an 8M and a 150M scale is a crucial finding. It demonstrates that our approach is robust and scalable, suggesting its viability for developing even larger hybrid models in the future.

While quantitative metrics for efficiency and stability are essential, the ultimate measure of a language model's success is the quality of the text it generates. To evaluate the practical capabilities of our hybrid architecture, we performed

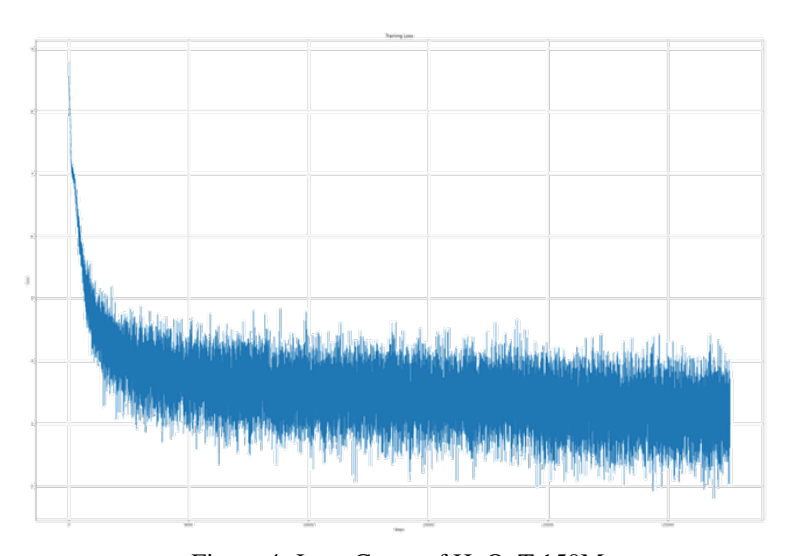


Figure 4: Loss Curve of HyQuT-150M

Technical Explanation

User

请为我讲解"大语言模型"这个概念。 (Please explain the concept of "Large Language Model".)

HvQuT-150M

大语言模型是一种常见的语言模型模型,它可以处理自然语言文本数据。它可以被用于各种不同的任务,例如文本分类、情感分析、机器翻译、问答系统等。大语言模型的训练是通过大量的训领域已经表现出了显著的成果,但它已经得得到广泛的发展和应用。

Conversational Ability

User

你更擅长哪一个学科? (Which subject are you best at?)

HyQuT-150M

作为一个人工智能助手,我没有自己的兴趣偏好,因此我不能说我最喜欢的学科。但是,我可以告诉你,我喜欢学习新事物,不断地挑战自己,不断学习新的知识和技能,以适应不同的工作环境和需求。同时,我也喜欢学习新知识和技能,以更好地适应新的工作环境和需求。

Figure 5: Qualitative Examples of Text Generated by the HyQuT-150M Model

a qualitative analysis of the text generated by the pre-trained HyQuT-150M model. The model was prompted with a variety of inputs designed to test its ability to handle different conversational and explanatory tasks.

Representative examples of the generated text are presented in Figure 5. The outputs demonstrate that the HyQuT-150M model successfully learns foundational language capabilities. It correctly interprets the user's intent, maintains contextual relevance, and generates multi-sentence responses that are coherent and on-topic.

5 Conclusion

In this work, we introduced HyQuT, the first hybrid quantum-classical large language model demonstrated to be capable of coherent, generative NLP. By successfully integrating a variational quantum circuit into Transformer architectures—implemented as HyQuT-8M and HyQuT-150M—our research bridges the gap between the theoretical promise of quantum computing and the practical demands of large-scale generative AI. This study moves beyond the established domain of quantum machine learning for classification and regression tasks, venturing into the more complex and challenging realm of language generation.

Our experimental results provide a strong proof-of-concept for the viability of this hybrid approach. We have shown that a remarkably compact quantum component—requiring only 10 qubits and approximately 80 quantum gates—can effectively replace over 10% of the classical parameters in a 150M-scale model. Crucially, this significant reduction in classical resources was achieved without compromising the model's training stability, as evidenced by its consistent loss convergence. The preservation of the model's core ability to generate contextually relevant text further underscores the feasibility of our framework.

While our findings are promising, we acknowledge that this work represents an initial but crucial step. A natural and important direction is to scale this methodology to larger and more capable architectures. Furthermore, investigating the integration of quantum modules into different model families could reveal new opportunities for efficiency gains. Ultimately, this research paves the way for a new paradigm of quantum-enhanced NLP, offering a potential path to mitigate the escalating computational demands of classical LLMs.

Acknowledgments

Part of this work is supposed by the Yangtze Delta Industrial Innovation Center of Quantum Science and Technology, Suzhou.

References

[1] Ashish Vaswani, Noam Shazeer, Niki Parmar, Jakob Uszkoreit, Llion Jones, Aidan N Gomez, Ł ukasz Kaiser, and Illia Polosukhin. Attention is all you need. In I. Guyon, U. Von Luxburg, S. Bengio, H. Wallach, R. Fergus, S. Vishwanathan, and R. Garnett, editors, *Advances in Neural Information Processing Systems*, volume 30. Curran Associates, Inc., 2017.

- [2] Alec Radford, Jeffrey Wu, Rewon Child, David Luan, Dario Amodei, Ilya Sutskever, et al. Language models are unsupervised multitask learners. *OpenAI blog*, 1(8):9, 2019.
- [3] Tom Brown, Benjamin Mann, Nick Ryder, Melanie Subbiah, Jared D Kaplan, Prafulla Dhariwal, Arvind Neelakantan, Pranav Shyam, Girish Sastry, Amanda Askell, et al. Language models are few-shot learners. *Advances in neural information processing systems*, 33:1877–1901, 2020.
- [4] Hugo Touvron, Thibaut Lavril, Gautier Izacard, Xavier Martinet, Marie-Anne Lachaux, Timothée Lacroix, Baptiste Rozière, Naman Goyal, Eric Hambro, Faisal Azhar, et al. Llama: Open and efficient foundation language models. *arXiv preprint arXiv:2302.13971*, 2023.
- [5] David Patterson, Joseph Gonzalez, Quoc Le, Chen Liang, Lluis-Miquel Munguia, Daniel Rothchild, David So, Maud Texier, and Jeff Dean. Carbon emissions and large neural network training. arXiv preprint arXiv:2104.10350, 2021.
- [6] Jacob Biamonte, Peter Wittek, Nicola Pancotti, Patrick Rebentrost, Nathan Wiebe, and Seth Lloyd. Quantum machine learning. *Nature*, 549(7671):195–202, 2017.
- [7] Jacob Devlin, Ming-Wei Chang, Kenton Lee, and Kristina Toutanova. Bert: Pre-training of deep bidirectional transformers for language understanding. In *Proceedings of the 2019 conference of the North American chapter of the association for computational linguistics: human language technologies, volume 1 (long and short papers)*, pages 4171–4186, 2019.
- [8] Jared Kaplan, Sam McCandlish, Tom Henighan, Tom B Brown, Benjamin Chess, Rewon Child, Scott Gray, Alec Radford, Jeffrey Wu, and Dario Amodei. Scaling laws for neural language models. *arXiv preprint* arXiv:2001.08361, 2020.
- [9] Long Ouyang, Jeffrey Wu, Xu Jiang, Diogo Almeida, Carroll Wainwright, Pamela Mishkin, Chong Zhang, Sandhini Agarwal, Katarina Slama, Alex Ray, et al. Training language models to follow instructions with human feedback. *Advances in neural information processing systems*, 35:27730–27744, 2022.
- [10] Paul F Christiano, Jan Leike, Tom Brown, Miljan Martic, Shane Legg, and Dario Amodei. Deep reinforcement learning from human preferences. *Advances in neural information processing systems*, 30, 2017.
- [11] Hugo Touvron, Louis Martin, Kevin Stone, Peter Albert, Amjad Almahairi, Yasmine Babaei, Nikolay Bashlykov, Soumya Batra, Prajjwal Bhargava, Shruti Bhosale, et al. Llama 2: Open foundation and fine-tuned chat models. *arXiv preprint arXiv:2307.09288*, 2023.
- [12] Edward J Hu, Yelong Shen, Phillip Wallis, Zeyuan Allen-Zhu, Yuanzhi Li, Shean Wang, Lu Wang, Weizhu Chen, et al. Lora: Low-rank adaptation of large language models. *ICLR*, 1(2):3, 2022.
- [13] Bob Coecke, Mehrnoosh Sadrzadeh, and Stephen Clark. Mathematical foundations for a compositional distributional model of meaning. *arXiv* preprint arXiv:1003.4394, 2010.
- [14] Guangxi Li, Xuanqiang Zhao, and Xin Wang. Quantum self-attention neural networks for text classification. *Science China Information Sciences*, 67(4):142501, 2024.
- [15] Hui Zhang, Qinglin Zhao, and Chuangtao Chen. A light-weight quantum self-attention model for classical data classification. *Applied Intelligence*, 54(4):3077–3091, 2024.
- [16] Jiachun Wei, Zhimin He, Chuangtao Chen, Maijie Deng, and Haozhen Situ. Povm-based quantum self-attention neural network. In 2023 International Conference on Wavelet Analysis and Pattern Recognition (ICWAPR), pages 117–122. IEEE, 2023.
- [17] Hui Zhang, Qinglin Zhao, Mengchu Zhou, and Li Feng. Hqvit: Hybrid quantum vision transformer for image classification. *arXiv preprint arXiv:2504.02730*, 2025.
- [18] Eyup B Unlu, Marçal Comajoan Cara, Gopal Ramesh Dahale, Zhongtian Dong, Roy T Forestano, Sergei Gleyzer, Daniel Justice, Kyoungchul Kong, Tom Magorsch, Konstantin T Matchev, et al. Hybrid quantum vision transformers for event classification in high energy physics. *Axioms*, 13(3):187, 2024.
- [19] Marçal Comajoan Cara, Gopal Ramesh Dahale, Zhongtian Dong, Roy T Forestano, Sergei Gleyzer, Daniel Justice, Kyoungchul Kong, Tom Magorsch, Konstantin T Matchev, Katia Matcheva, et al. Quantum vision transformers for quark–gluon classification. *Axioms*, 13(5):323, 2024.
- [20] Sanjay Chakraborty and Fredrik Heintz. Integrating quantum-classical attention in patch transformers for enhanced time series forecasting. *arXiv* preprint arXiv:2504.00068, 2025.
- [21] Siddhant Dutta, Nouhaila Innan, Alberto Marchisio, Sadok Ben Yahia, and Muhammad Shafique. Qadqn: Quantum attention deep q-network for financial market prediction. In 2024 IEEE International Conference on Quantum Computing and Engineering (QCE), volume 2, pages 341–346. IEEE, 2024.

- [22] Jinjing Shi, Ren-Xin Zhao, Wenxuan Wang, Shichao Zhang, and Xuelong Li. Qsan: A near-term achievable quantum self-attention network. *IEEE Transactions on Neural Networks and Learning Systems*, 2024.
- [23] Fu Chen, Qinglin Zhao, Li Feng, Longfei Tang, Yangbin Lin, and Haitao Huang. Quantum complex-valued self-attention model. *arXiv preprint arXiv:2503.19002*, 2025.
- [24] Iordanis Kerenidis, Natansh Mathur, Jonas Landman, Martin Strahm, Yun Yvonna Li, et al. Quantum vision transformers. *Quantum*, 8:1265, 2024.
- [25] Jiangshu Technology (DeepCtrl). DeepCtrl Supervised Fine-Tuning (SFT) Dataset. ModelScope, 2025. [Online]. Available: https://www.modelscope.cn/datasets/deepctrl/deepctrl-sft-data. (Accessed on: Oct. 31, 2025).

A Detailed Parameter Breakdown of the HyQuT-8M Model

Table 4: Layer-by-layer parameter distribution of the HyQuT-8M model.

Model Layer Name	Dimensions	Parameter Count	Memory (MB)			
model.embed_tokens.embedding_table	(6401, 512)	3,277,312	12.50			
Transformer Layer Block (Structure repeats for 2 layers)						
layers.N.input_layernorm.weight	(512,)	512	< 0.01			
layers.N.self_attn.q_proj.weight	(512, 512)	262,144	1.00			
layers.N.self_attn.k_proj.weight	(128, 512)	65,536	0.25			
layers.N.self_attn.v_proj.weight	(128, 512)	65,536	0.25			
layers.N.self_attn.o_proj.weight	(512, 512)	262,144	1.00			
layers.N.post_attention_layernorm.weight	(512,)	512	< 0.01			
layers.N.mlp.gate_proj.* (Hybrid Module)reduce_proj.weightreduce_proj.biasmq_layers.0.weight (Quantum Params)dense_expand.weightdense_expand.bias layers.N.mlp.down_proj.weight	(20, 512) (20,) (40,) (1024, 1) (1024,) (512, 1024)	10,240 20 40 1,024 1,024 524,288	0.04 <0.01 <0.01 <0.01 <0.01 <0.01			
layers.N.mlp.down_proj.bias	(512,)	512	< 0.01			
layers.N.mlp.up_proj.weight	(1024, 512)	524,288	2.00			
layers.N.mlp.up_proj.bias	(1024,)	1,024	< 0.01			
End of Transformer Layer Block						
model.norm.weight	(512,)	512	< 0.01			
lm_head.bias	(6401,)	6,401	0.02			
Total	-	6,721,913	25.64 MB			

^{*}Note: The mlp.gate_proj block details the components of our Hybrid Quantum Module. mq_layers.0.weight represents the trainable parameters θ of the VQC.